

Chaoticity parameter λ in two-pion interferometry in an expanding boson gas model

Jie Liu, Peng Ru, Wei-Ning Zhang*

*School of physics and optoelectronic technology,
Dalian University of Technology, Dalian, Liaoning 116024, China*

Cheuk-Yin Wong

*Physics Division, Oak Ridge National Laboratory,
Oak Ridge, Tennessee 37831, USA*

Abstract

We investigate the chaoticity parameter λ in two-pion interferometry in an expanding boson gas model. The degree of Bose-Einstein condensation of identical pions, density distributions, and Hanbury-Brown-Twiss (HBT) correlation functions are calculated for the expanding gas within the mean-field description with a harmonic oscillator potential. The results indicate that a sources with thousands of identical pions may exhibit a degree of Bose-Einstein condensation at the temperatures during the hadronic phase in relativistic heavy-ion collisions. This finite condensation may decrease the chaoticity parameter λ in the two-pion interferometry measurements at low pion pair momenta, but influence only slightly the λ value at high pion pair momentum.

PACS numbers: 25.75.Gz, 05.30.Jp

* wnzhang@dlut.edu.cn

I. INTRODUCTION

Hanbury-Brown-Twiss (HBT) interferometry is a useful tool to study the space-time structure of the particle-emitting source, through the two-particle momentum correlation function of identical bosons [1–5]. In HBT interferometry, the chaoticity parameter λ is introduced phenomenologically to represent the intercept of the correlation function at zero relative momentum of the particle pair. The value of λ is related to the degree of source coherence, as it is well known that HBT correlation disappears for a completely coherent source.

In high energy heavy-ion collisions, pions are the most copiously produced particles. The use of two-pion interferometry to probe the source coherence was proposed at the end of 1970s [1, 6]. However, the experimental measurement of the λ quantity is affected by the presence of many other effects such as particle misidentification, long-live resonance decay, final state Coulomb interaction, non-Gaussian source distribution, and so on [3, 5]. The explanation of the experimental λ results is still an open question. In 1993, S. Pratt proposed a pion laser model in high energy collisions and studied the influence of pion laser on two-pion HBT correlation function and the chaoticity parameter [7]. In 1998, T. Csörgő and J. Zimányi investigated the effect of Bose-Einstein condensation on two-pion interferometry [8]. They utilized Gaussian formulas describing the space and momentum distributions of a static non-relativistic boson system, and investigated the influence of the condensation on pion multiplicity distribution. In 2007, C. Y. Wong and W. N. Zhang studied the dependence of the HBT chaoticity parameter on the degree of Bose-Einstein condensation for static non-relativistic and relativistic boson gases within a mean-field with a spherical harmonic oscillator potential [9], which can be analytically solved in non-relativistic case and be used in atomic physics [10–12]. The similar work for cylindrical static boson gas sources was just completed [13]. Recently, the experimental investigation of the source coherence in the Pb-Pb collisions at $\sqrt{s_{NN}} = 2.76$ TeV at the Large Hadron Collider (LHC) was carried out by the ALICE collaboration [14]. A substantial degree of source coherence was measured [14], using a new three-pion interferometry technique with an improvement over the past efforts [15–17]. It is of interest to study the reasons of source coherence in heavy-ion collisions at the LHC energy.

In this article we investigate the Bose-Einstein condensation of identical pions for an

expanding relativistic gas source within the time-dependent mean-field of harmonic oscillator potential, which decreases with time in the temperature region of the hadronic phase, 170–60 MeV, in relativistic heavy-ion collisions. Using one- and two-body density matrices, we calculate the pion space and momentum density distributions, HBT correlation functions, and the chaoticity parameter λ in HBT interferometry in the temperature region of 60 to 170 MeV. The influences of the pion source Bose-Einstein condensation on the λ values in the HBT measurements at different pion pair momenta and temperatures are investigated. The results indicate that a source with thousands of identical pions may appear to possess a substantial degree of Bose-Einstein condensation. The finite condensation may decrease the chaoticity parameter λ in the two-pion interferometry measurements at low pion pair momenta, but influence only slightly the λ value measured at high pion pair momenta. In heavy-ion central collisions at the LHC energy, the identical pion multiplicity of event can reach several thousands. In this case, the effects of Bose-Einstein condensation on the chaoticity parameters in two-pion and multi-pion HBT measurements would be of great interest.

This paper is organized as follows. In Sec. II, we investigate pion Bose-Einstein condensation for the expanding sources of boson gas in relativistic heavy-ion collision environments. In Sec. III, we calculate the pion space and momentum density distributions and two-pion HBT correlation functions, using one- and two-body density matrices. We investigate the influences of the Bose-Einstein condensation on the chaoticity parameter in two-pion interferometry in Sec. IV. Finally, summary and conclusion are present in Sec. V.

II. BOSE-EINSTEIN CONDENSATION IN EXPANDING BOSON GAS WITH HARMONIC OSCILLATOR POTENTIAL

A. Time-dependent harmonic oscillator potential

Base on the previous works of boson gases trapped by a static harmonic oscillator potential in atomic physics and high energy heavy-ion collisions [9–11, 13], we are interesting in the study of the boson gas of identical pions within a time-dependent harmonic oscillator potential, $V(\mathbf{r}, t)$, that arises approximately from the mean-field of the hadronic medium in high energy heavy-ion collisions [9]. The time-dependent harmonic oscillator potential is

given by,

$$V(\mathbf{r}, t) = \frac{1}{2} m \omega^2(t) r^2 = \frac{1}{2} \hbar \omega(t) \frac{r^2}{a^2(t)}, \quad (1)$$

where, t is source evolution time, m is the boson mass, $\hbar\omega(t)$ measures the time-dependent potential strength, and the characteristic length of harmonic oscillator a is defined as $a(t) = \sqrt{\hbar/m\omega(t)}$. We assume that the characteristic length is proportional to a parameterized source radius which increases with time as $R = R_0 + \alpha t$, where R_0 is the initial radius of source and α is a parameter related to the source average expansion velocity and will be determined by hydrodynamics. For ideal boson gas, the system energy is simply the summation of all individual bosons, and the energy levels of a boson for given $\hbar\omega$ are

$$\varepsilon_n = n\hbar\omega + \frac{3}{2}\hbar\omega, \quad n = 0, 1, 2, \dots \quad (2)$$

The degeneracy of ε_n is $g_n = (n + 1)(n + 2)/2$.

Assuming the relaxation time of system is smaller than the source evolution time, we may approximately deal with the expansion gas as uniform system at each evolution time, as a first-step improvement to static treatment in the approximation of a quasi-static adiabatic process. For such a quasi-static adiabatic expansion of an ideal gas, the system temperature T and the volume V have the relationship $TV^{\gamma-1} = \text{constant}$, where γ is the ratio of the specific heats at constant pressure and volume. For example, γ is 5/3 for non-relativistic monatomic gas. For our problem, we seek a relation between T and the size of an expanding hadron gas system from relativistic hydrodynamics in high energy heavy-ion collisions. We shows in Figure 1 the temperature T averaged over radial coordinate r , $\langle T(t, r) \rangle_r$, obtained from the relativistic hydrodynamic evolution of a spherical source with an initial radius $R_0 = 6$ fm and an initial temperature $T_0 = 170$ MeV. For the spherical source, we find that the system temperature satisfies

$$T = \frac{T_0 R_0^\delta}{R^\delta} = \frac{T_0 R_0^\delta}{(R_0 + \alpha t)^\delta}. \quad (3)$$

The fitted line in Fig. 1 corresponds to the above formula (3) with $\alpha = 0.62$ and $\delta = 1.88$. We shall use this parameterized formula of the temperature as determined by relativistic hydrodynamics in our calculations and shall take the characteristic length a in Eq. (1) as,

$$a = C_1(R_0 + \alpha t), \quad (4)$$

where C_1 is a proportional parameter. It will be seen that the results of source root-mean-squared radius are sensitive to the parameter C_1 . So, they may provide a restriction to C_1

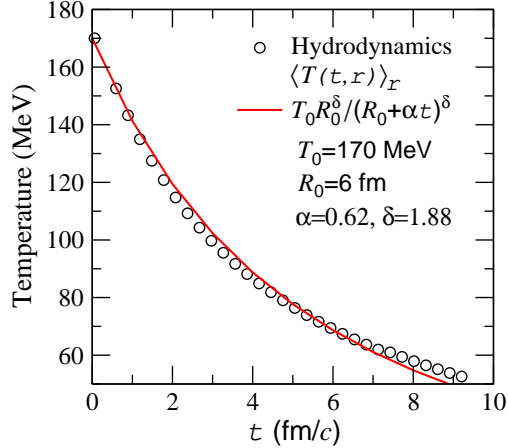


FIG. 1: (Color online) Source temperature as a function of evolution time.

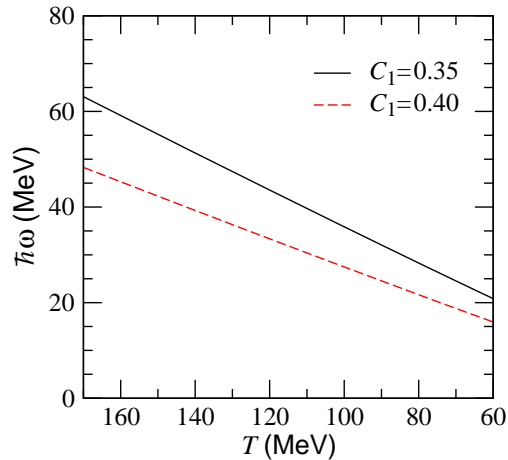


FIG. 2: (Color online) Potential strength of harmonic oscillator as a function of temperature.

value. We plot in Fig. 2 the strength of harmonic oscillator potential, $\hbar\omega$, as a function of temperature for $C_1 = 0.35$ and 0.40 , respectively. The potential strength decreases with evolution time for the expanding source, and thus decreases with decreasing temperature.

B. Pion Bose-Einstein condensation

In relativistic heavy-ion collisions, the source temperature of hadron gas phase is in the region of [60 to 170] MeV. At these temperatures pion motion is relativistic. For a quasi-static process, at each time stage the system is treated as a static state, and the eigenvalue

equation for relativistic pion with only a scalar interaction as in Eq. (1) is given by [9]

$$\left[\frac{\mathbf{p}^2}{2m} + V(\mathbf{r}) \right] U(\mathbf{r}) = \frac{E^2 - m^2}{2m} U(\mathbf{r}) = \varepsilon U(\mathbf{r}). \quad (5)$$

Here the potential $V(\mathbf{r})$ is given by Eq. (1) at each time stage, for instance at $t = t_1, t_2, \dots, t_m$, $V(\mathbf{r}) = \hbar\omega(t_1) r^2/[2a^2(t_1)], \hbar\omega(t_2) r^2/[2a^2(t_2)], \dots, \hbar\omega(t_m) r^2/[2a^2(t_m)]$. The eigenenergy of the relativistic pion is

$$E_n = \sqrt{m^2 + 2m\varepsilon_n}, \quad (6)$$

where $\varepsilon_n = (n + 3/2)\hbar\omega$, $n = 0, 1, 2, \dots$, and the eigenfunction is

$$U_n(\mathbf{r}) = N_{n_r, l} \left(\frac{r}{a} \right)^l e^{-\frac{r^2}{2a^2}} L_{n_r}^{l+\frac{1}{2}} \left(\frac{r^2}{a^2} \right) Y_{lm}(\theta, \varphi), \quad (7)$$

where, $n = 2n_r + l$,

$$N_{n_r, l} = \left[\frac{2n!}{a^3 \Gamma(n_r + l + \frac{3}{2})} \right]^{1/2}, \quad (8)$$

L and Y are Laguerre polynomial and spherical harmonics, respectively. The eigenfunction of the ground state is

$$U_0(\mathbf{r}) = \left(\frac{1}{a^2 \pi} \right)^{3/4} e^{-\frac{r^2}{2a^2}}. \quad (9)$$

For a quasi-static expansion, ω or a is a function of the evolution time.

We introduce \tilde{E}_n to measure the relative energy levels to the energy of the $n = 0$ state,

$$\tilde{E}_n = E_n - \sqrt{m^2 + 2m \times \frac{3}{2} \hbar\omega}. \quad (10)$$

For the identical boson gas with a fixed number of particles, N , and at a given temperature $T = 1/\beta$, we have

$$N = N_0 + N_T, \quad (11)$$

where, N_0 is the number of condensate particles in $n = 0$ state,

$$N_0 = \frac{\mathcal{Z}}{1 - \mathcal{Z}}, \quad (12)$$

N_T is the number of the particles in $n > 0$ states,

$$N_T = \sum_{n>0}^{\infty} \frac{g_n \mathcal{Z} e^{-\beta \tilde{E}_n}}{1 - \mathcal{Z} e^{-\beta \tilde{E}_n}}, \quad (13)$$

and \mathcal{Z} is the fugacity parameter which includes the factor for the lowest energy ε_0 [9, 11]. Because $N_0 \geq 0$, the values of \mathcal{Z} are between zero and one. When temperature is lowered

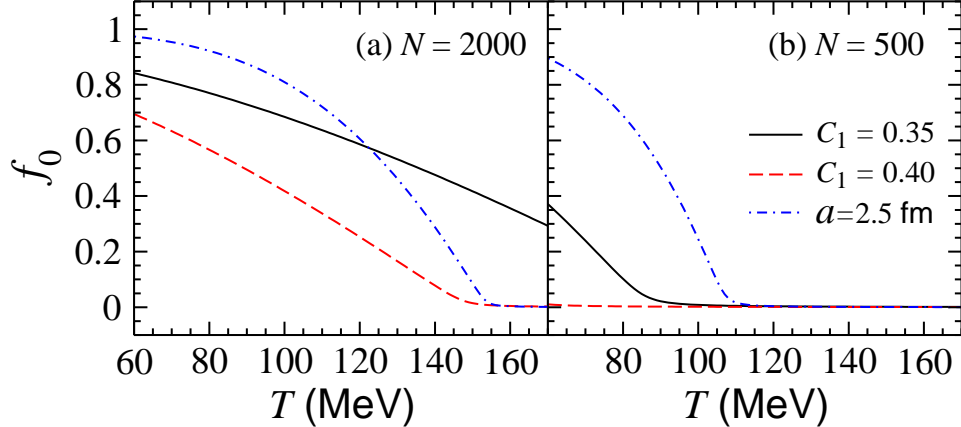


FIG. 3: (Color online) Source condensation fraction as a function of temperature.

below the critical temperature T_c , Bose-Einstein condensation occurs. In this case, $N_0 \sim N$ and $\mathcal{Z} \sim N/(N+1)$.

From Eqs. (11), (12), and (13), one can calculate the fugacity parameter \mathcal{Z} for fixed N numerically, and then obtain the condensation fraction [9, 13],

$$f_0 = \frac{N_0}{N} = \frac{\mathcal{Z}}{(1-\mathcal{Z})N}. \quad (14)$$

In Figs. 3(a) and 3(b), we show the condensation fraction for the sources with $N = 2000$ and 500, respectively. Here, the solid and dashed lines are for the proportional parameter C_1 in Eq. (4) being taken as 0.35 and 0.40, and the dashed-dot lines are for the static source with a fixed characteristic length $a = 2.5$ fm ($R = R_0 = 6$ fm, $C_1 = 0.417$) for comparison. One can see that the condensation fraction f_0 decreases with increasing temperature. In Fig. 3(a), the values of f_0 for the $C_1 = 0.40$ case and for the fixed a case both approach zero at $T \sim 160$ MeV, corresponding to the completely uncondensed case. However, the condensation fraction for $C_1 = 0.35$ is finite at the initial high temperature for the source with $N = 2000$. For the expanding sources f_0 increases more slowly with decreasing temperature than that for the static source. From Fig. 3(b) it can be seen that the expanding source with $N = 500$ and $C_1 = 0.35$ has only a small condensation fraction at low temperatures, and the system with $C_1 = 0.40$ is uncondensed in the whole temperature region.

III. DENSITY DISTRIBUTIONS AND CORRELATION FUNCTIONS

Based on quantum statistics, the spatial one-body density matrix for the boson gas with given particle number and temperature is

$$G^{(1)}(\mathbf{r}_1, \mathbf{r}_2) = \sum_{n=0}^{\infty} U_n^*(\mathbf{r}_1) U_n(\mathbf{r}_2) \frac{g_n \mathcal{Z} e^{-\beta \tilde{E}_n}}{1 - \mathcal{Z} e^{-\beta \tilde{E}_n}}, \quad (15)$$

and the density matrix in momentum space is

$$G^{(1)}(\mathbf{p}_1, \mathbf{p}_2) = \sum_{n=0}^{\infty} U_n^*(\mathbf{p}_1) U_n(\mathbf{p}_2) \frac{g_n \mathcal{Z} e^{-\beta \tilde{E}_n}}{1 - \mathcal{Z} e^{-\beta \tilde{E}_n}}, \quad (16)$$

where $U_n(\mathbf{p})$ are the eigenfunctions in momentum space, which have the exchange symmetry $\mathbf{p}a/\hbar - \mathbf{r}/a$ with the spatial eigenfunctions $U_n(\mathbf{r})$ [Eqs. (7) and (9)] for harmonic oscillator potential.

In the limit of a large number of particles, $N(N-1) \sim N^2 (\gg N_T, N_0)$, the two-body density matrices can be written as [9–11]

$$G^{(2)}(\mathbf{r}_1, \mathbf{r}_2; \mathbf{r}_1, \mathbf{r}_2) = G^{(1)}(\mathbf{r}_1, \mathbf{r}_1) G^{(1)}(\mathbf{r}_2, \mathbf{r}_2) + |G^{(1)}(\mathbf{r}_1, \mathbf{r}_2)|^2 - N_0^2 |U_0(\mathbf{r}_1)|^2 |U_0(\mathbf{r}_2)|^2, \quad (17)$$

$$G^{(2)}(\mathbf{p}_1, \mathbf{p}_2; \mathbf{p}_1, \mathbf{p}_2) = G^{(1)}(\mathbf{p}_1, \mathbf{p}_1) G^{(1)}(\mathbf{p}_2, \mathbf{p}_2) + |G^{(1)}(\mathbf{p}_1, \mathbf{p}_2)|^2 - N_0^2 |U_0(\mathbf{p}_1)|^2 |U_0(\mathbf{p}_2)|^2. \quad (18)$$

A. Density distributions

With density matrices, we can obtain the density distributions in configuration and momentum spaces as

$$\rho(\mathbf{r}) = G^{(1)}(\mathbf{r}, \mathbf{r}) = \sum_{n=0}^{\infty} \frac{g_n \mathcal{Z} e^{-\beta \tilde{E}_n}}{1 - \mathcal{Z} e^{-\beta \tilde{E}_n}} |U_n(\mathbf{r})|^2, \quad (19)$$

$$\rho(\mathbf{p}) = G^{(1)}(\mathbf{p}, \mathbf{p}) = \sum_{n=0}^{\infty} \frac{g_n \mathcal{Z} e^{-\beta \tilde{E}_n}}{1 - \mathcal{Z} e^{-\beta \tilde{E}_n}} |U_n(\mathbf{p})|^2. \quad (20)$$

In Figs. 4(a) and 4(b) we plot the spatial density distributions of the expanding sources with $C_1 = 0.35$ and 0.40 , and at different temperatures, respectively. In Fig. 4(c) we plot the spatial density distributions of the static source with $a = 2.5$ fm for comparison. The particle number of the systems is 2000. At $T = 160$ MeV, the distribution for $C_1 = 0.35$ has

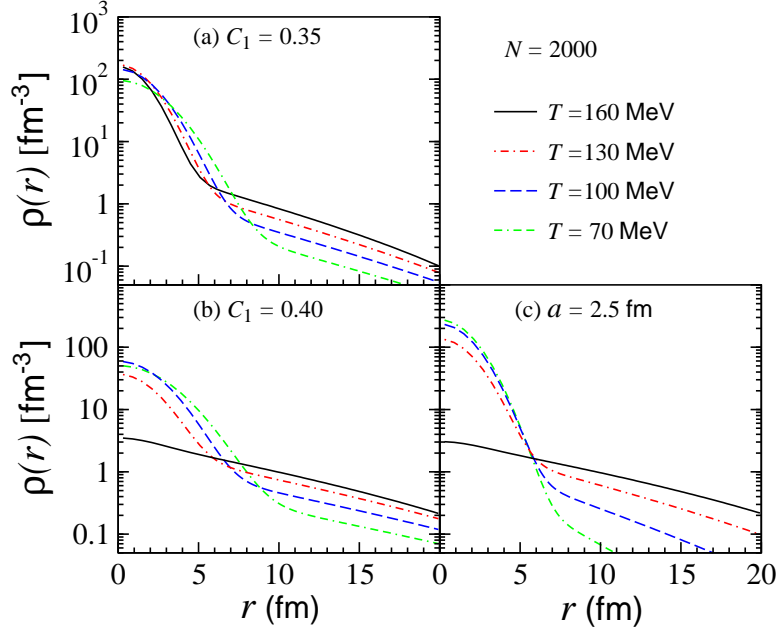


FIG. 4: (Color online) Spatial density distributions of the expanding sources with $C_1 = 0.35$ and 0.40 , and the system with fixed $a = 2.5$ fm. The particle number of the systems is 2000.

an obvious rise in the small r region as compared to those for $C_1 = 0.40$ and $a = 2.5$ fm. This is because the source with $C_1 = 0.35$ has a finite degree of Bose-Einstein condensation at $T = 160$ MeV, and the other systems are completely uncondensed at this temperature (see Fig. 3). Similarly, one can see the two-tiered structure of the density distributions caused by the condensation for all the three systems at the lower temperatures. Because the source with $C_1 = 0.40$ has lower condensation fraction at the lower temperatures, its corresponding density distributions are wider than those of the other systems.

In Fig. 5, we plot the density distributions in momentum space for the expanding sources with $N = 2000$ and 500 . One can also see the two-tiered structure in the momentum density distributions in Figs. 5(a), 5(b), and 5(c), arising from the Bose-Einstein condensation at lower temperatures. The average particle momentum is lower for the source with a higher degree of condensation. For the completely uncondensed source in Fig. 5(d), there is no two-tiered structure of momentum density distribution in the whole temperature region. The momentum density distribution becomes wider when the temperature increases.

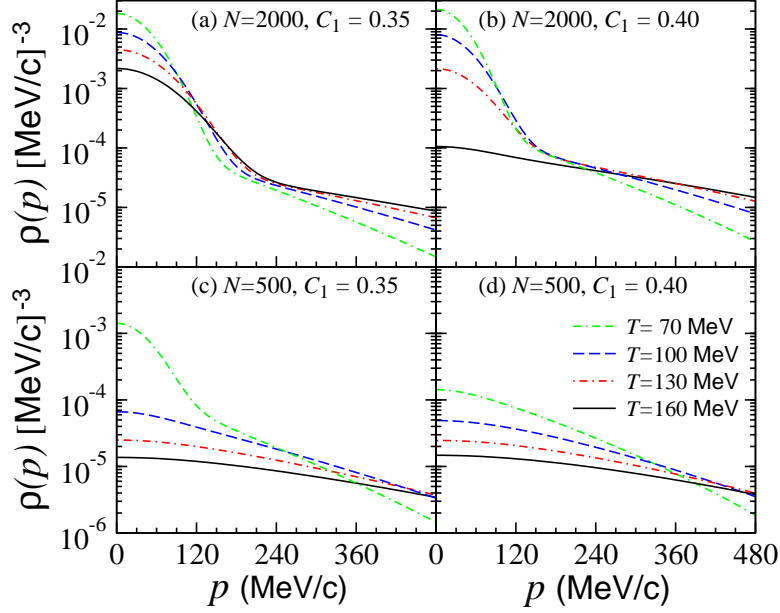


FIG. 5: (Color online) The density distributions in momentum space for the expanding sources with $N = 2000$ and 500 , and at different temperatures.

B. Two-particle momentum correlation functions

Using density matrices, the two-particle correlation function in momentum space can be written as

$$C(\mathbf{p}_1, \mathbf{p}_2) = \frac{G^{(2)}(\mathbf{p}_1, \mathbf{p}_2; \mathbf{p}_1, \mathbf{p}_2)}{G^{(1)}(\mathbf{p}_1, \mathbf{p}_1) G^{(1)}(\mathbf{p}_2, \mathbf{p}_2)}. \quad (21)$$

From Eq. (18), we have

$$C(\mathbf{p}_1, \mathbf{p}_2) = 1 + \frac{|G^{(1)}(\mathbf{p}_1, \mathbf{p}_2)|^2 - N_0^2 |U_0(\mathbf{p}_1)|^2 |U_0(\mathbf{p}_2)|^2}{G^{(1)}(\mathbf{p}_1, \mathbf{p}_1) G^{(1)}(\mathbf{p}_2, \mathbf{p}_2)}. \quad (22)$$

In the nearly completely coherent case with almost all particles in the ground condensate state, $N_0 \rightarrow N$, the two terms in the numerator cancel each other and we have $C(\mathbf{p}_1, \mathbf{p}_2) = 1$, as it should be. For the other extreme of a completely chaotic system with $N_0 \ll N$, the second term in the numerator can be neglected and we have the usual one for a completely chaotic source,

$$C(\mathbf{p}_1, \mathbf{p}_2) = 1 + \frac{|G^{(1)}(\mathbf{p}_1, \mathbf{p}_2)|^2}{G^{(1)}(\mathbf{p}_1, \mathbf{p}_1) G^{(1)}(\mathbf{p}_2, \mathbf{p}_2)}. \quad (23)$$

It is convenient in interferometry analyses to introduce the average and relative momenta

$$\mathbf{p} = (\mathbf{p}_1 + \mathbf{p}_2)/2, \quad \mathbf{q} = \mathbf{p}_1 - \mathbf{p}_2. \quad (24)$$

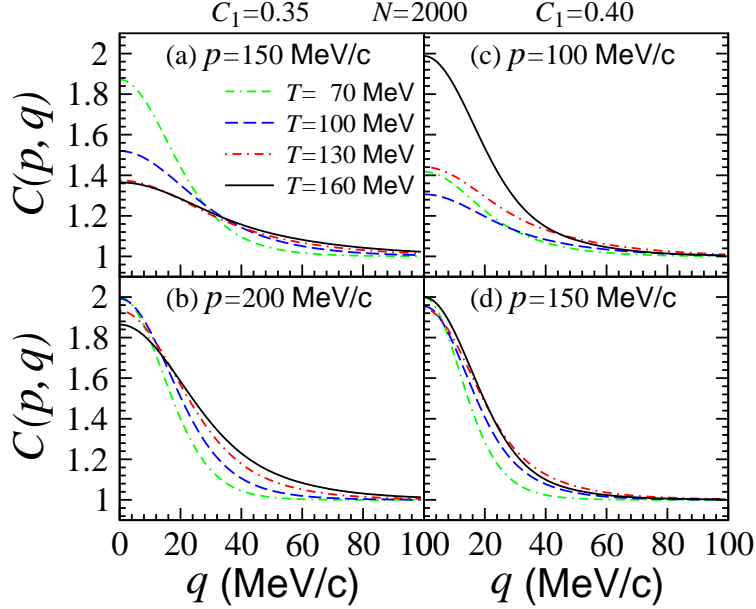


FIG. 6: (Color online) The two-pion correlation functions $C(p, q)$ for the sources with $N = 2000$, $C_1 = 0.35$ and 0.40 .

The momentum correlation function can be expressed alternatively in terms of the kinematic variables, \mathbf{p} and \mathbf{q} , and the correlation function $C(p, q)$ can be obtained in numerical calculations by integrating \mathbf{p}_1 and \mathbf{p}_2 in Eq. (22) for certain (p, q) bins.

In Fig. 6 we plot the two-pion correlation functions $C(p, q)$ for the sources with $N = 2000$, $C_1 = 0.35$ and 0.40 . One can see that at the higher momenta, $p = 200$ MeV for $C_1 = 0.35$ [Fig. 6(b)] and $p = 150$ MeV for $C_1 = 0.40$ [Fig. 6(d)], the width of the correlation functions decrease when the temperature decreases. This is because the source expansion leads to a decrease temperature. The intercepts of the correlation functions at the higher momenta are larger than the corresponding results at the lower momenta [Figs. 6(a) and 6(c)] because the particles with large momenta are from the uncondensed chaotic states on the average, for the finite condensation sources. One can also see from Figs. 6(a) and 6(c) that at the lower momenta the intercept varies with temperature in a non-monotonic manner. It will be discussed in detail in next section that the complexity of this variation arises because the intercept value depends not only on the condensation fraction but also on the radius of expanding source, both varying with temperature.

In actual interferometry analyses, the source expansion may lead to a space-momentum correlation so that the two particles with small relative momentum are from neighboring

source points [5, 18, 19]. This space-momentum correlation can influence the construction of HBT correlation functions and therefore the dependence of HBT radius as a function of particle pair momentum [5, 18, 19]. Note that the HBT correlation functions calculated by the density matrices has not included the effect of the space-momentum correlation. So, it is hard to compare the HBT radii obtained from the correlation functions calculated here with those from the actual interferometry analyses for expanding sources. However, the effect of Bose-Einstein condensation on the chaoticity parameter λ in HBT interferometry should be independent of this space-momentum correlation in principle, because the source condensation depends only on the source thermal environment.

IV. CHAOTICITY PARAMETER λ IN TWO-PION INTERFEROMETRY

In HBT analyses the chaoticity parameter λ is introduced phenomenologically to represent the intercept of the HBT correlation function at zero relative momenta of the particle pair,

$$\lambda(\mathbf{p}) = C(\mathbf{p}, \mathbf{q} = 0) - 1. \quad (25)$$

From Eq. (22), the chaoticity parameter can be expressed in terms of $N_0 = f_0 N$ and the ratio of the squared of ground state wave function $U_0(\mathbf{p})$ to the momentum density $\rho(\mathbf{p}) = G^{(1)}(\mathbf{p}, \mathbf{p})$,

$$\lambda(\mathbf{p}) = 1 - N_0^2 [|U_0(\mathbf{p})|^2 / \rho(\mathbf{p})]^2 \equiv 1 - [f_0 F_N(\mathbf{p})]^2, \quad (26)$$

where

$$F_N(\mathbf{p}) = N |U_0(\mathbf{p})|^2 / \rho(\mathbf{p}). \quad (27)$$

$F_N(p)$ gives the relative probability of particle pairs from the condensed state with momentum p to the momentum density. For the source with a finite condensation, $F_N(p)$ at large p will decrease as the momentum p increases because $|U_0(p)|^2$ decrease more rapidly than $\rho(p)$ as p increases.

In Fig. 7, we plot F_N as a function of momentum at different temperatures for the sources with $N = 2000$ and 500. From Fig. 7(a) one can see that the variation of F_N with momentum has an obvious abruptly changing point. For example, the curve of F_N for $T = 160$ MeV in Fig. 7(a) decreases more rapidly at $p \sim 200$ MeV/ c . The reason is that the density distribution $\rho(p)$ changes abruptly as a function of momentum at $p \sim 200$

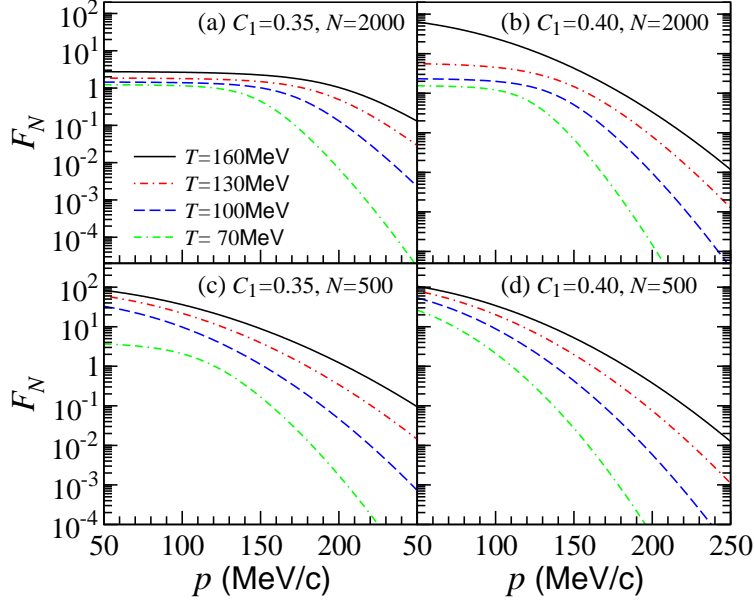


FIG. 7: (Color online) F_N as a function of momentum for the systems with $N = 2000$ and 500 , $C_1 = 0.35$ and 4.0 , and at different temperatures.

MeV/c [see Fig. 5(a)] for the source with a finite condensation fraction f_0 [see Fig. 3(a)]. With decreasing temperature, f_0 increases, and the changing point of momentum of $F_N(p)$ decreases. The values of F_N at small momentum decrease with decreasing temperature. This is because when the temperature decreases the characteristic length a increases, leading to the decrease of $|U_0(p)|^2$, and $\rho(p)$ is higher at small momentum for the lower temperature. For the completely uncondensed cases, for example, for the $T = 160$ MeV case in Fig. 7(b), the $T = 160, 130$, and 100 MeV cases in Fig. 7(c), and all cases in Fig. 7(d), there are no abruptly change points in F_N as the momentum increases. The values of F_N increase with temperature because the distribution of $\rho(p)$ becomes wider for the source with a smaller radius when the system is at higher temperature.

In Fig. 8, we plot the chaoticity parameter λ as a function of temperature T for different pair momentum values. For the source with $N = 2000$ and $C_1 = 0.35$, at $T = 170$ MeV in Fig. 8(a), the λ values are less than one and they increase with increasing momentum p . This is because that the source has a finite but small condensation fraction at that temperature, and the particles with large momenta are from the higher-energy uncondensed states on the average. When the temperature decreases, the condensation fraction f_0 increases but F_N decreases especially at large momentum. The competition of f_0 and F_N results in the value

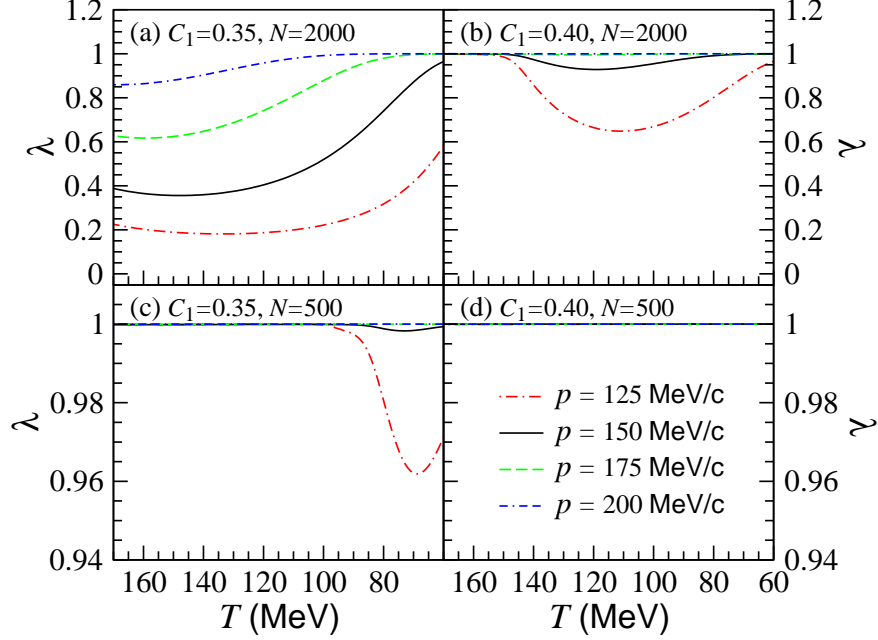


FIG. 8: (Color online) The chaoticity parameter λ as a function of temperature for different pion pair momentum values.

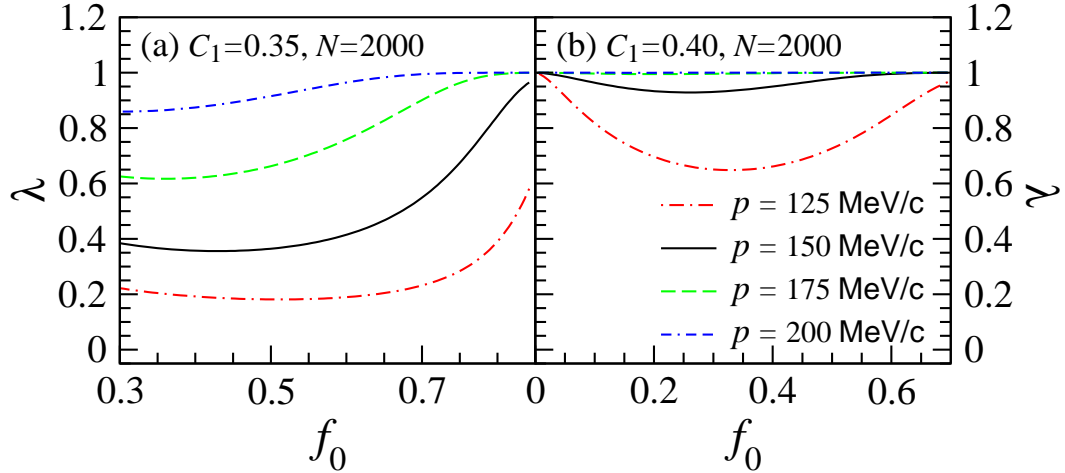


FIG. 9: (Color online) The chaoticity parameter λ as a function of f_0 for different pion pair momentum values and $N = 2000$.

of λ as a function of temperature. In Fig. 8(b), the λ value is one at temperatures greater than 150 MeV because the source is completely uncondensed at these temperatures, and thus $f_0 = 0$. For the smaller particle number source in Figs. 8(c) and 8(d), one can see that the λ results deviate from one only for small momenta and at low temperatures. The

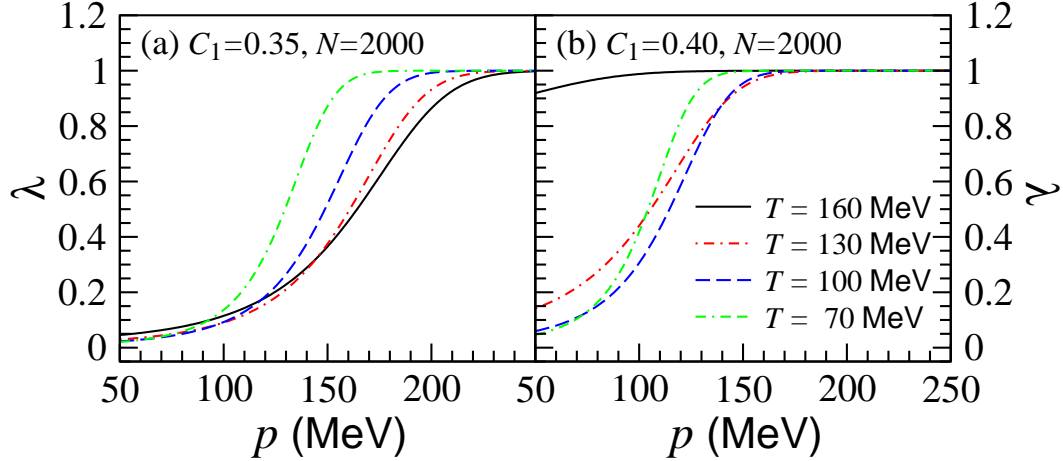


FIG. 10: (Color online) The chaotic parameter λ as a function of pion pair momentum at different temperatures.

chaoticity parameter results in Fig. 8(a) and Fig. 8(b) are consistent with the intercepts of the two-pion correlation functions shown in Fig. 6. Figures 9(a) and 9(b) show the variation of λ with the condensation fraction f_0 for the source with $N = 2000$, $C_1 = 0.35$ and 0.40 , respectively. The appearances of the curves are similar to those shown in Figs. 8(a) and 8(b) because f_0 varies almost linearly with temperature for the expanding sources [see the solid and dashed lines in Fig. 3(a)]. The variation of λ with f_0 is different from the results of the static source where λ decreases with f_0 monotonically (see the Fig. 11 in Ref. [13]).

In Fig. 10, we plot the chaotic parameter λ as a function of the momentum at different temperatures for the sources with $N = 2000$. The values of λ increase with increasing momentum and approach to one at high momenta because the particles with large momenta are from the uncondensed high-energy states on the average, for the sources with a finite and small condensation fraction. For an expanding source, $U_0(p)$ is also a function of the temperature because the characteristic length a increases when the temperature decreases. So, the increases of λ with the momentum at different temperatures exhibit more complexity than the results for the static source (see the Fig. 16 in Ref. [13]).

In the heavy-ion collisions at the LHC energy, the identical pion multiplicity of event can reach several thousands. The calculations indicate that in this case the effect of Bose-Einstein condensation on the chaotic parameter λ in two-pion HBT interferometry may be considerable and should be taken into account. In Fig. 11 we plot the root-mean-squared radius (RMSR) of the source with $N = 2000$, $C_1 = 0.35$ and 4.0 . It can be seen that the

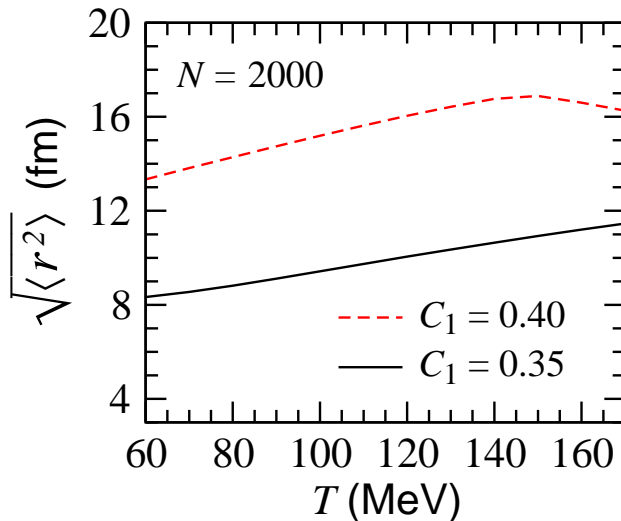


FIG. 11: (Color online) The root-mean-squared radius of the sources with $N = 2000$, $C_1 = 0.35$ and 0.40.

results of the RMSR are much sensitive to the parameter C_1 . Considering the RMSR of the sources in Pb-Pb collisions at the LHC to be of the order 10 fm, the values of parameter C_1 between 0.35 and 0.40 appear reasonable.

V. SUMMARY AND CONCLUSION

We investigate pion gas Bose-Einstein condensation in relativistic heavy-ion collisions in an expanding source model. The relationship between the source temperature and radius is given by a parameterized formula obtained with relativistic hydrodynamic calculations. Using the one- and two-body density matrices for the boson gas within the mean-field with a harmonic oscillator potential, we calculate the space and momentum density distributions, two-pion HBT correlation function, and the chaoticity parameter in two-pion interferometry for the identical pion sources at the temperatures of the hadronic phase in relativistic heavy-ion collisions. The influences of the source particle number and the potential strength of mean-field on the density distributions, HBT correlation functions, and λ values are discussed.

In the heavy-ion collisions at the LHC energy, the identical pion multiplicity of event can reach several thousands. Our investigations indicate that the sources with thousands of

identical pions may exhibit a degree of Bose-Einstein condensation at the temperatures of the hadronic phase, 170–60 MeV, in relativistic heavy-ion collisions. This finite condensation may decrease the chaoticity parameter λ in the two-pion interferometry measurements at low pion pair momenta, and influence very slightly the λ value at high pion pair momentum. Unlike the results of static source, the chaoticity parameter λ for the expanding source depends not just on the condensation fraction f_0 alone. Its variation with the temperature is more complicated. In experiments, the source temperature can be measured by the slope of momentum spectrum. Once the temperature is determined, it is of interest to compare the model λ values with experimental HBT data at different momenta.

In this paper we investigate the influence of Bose-Einstein condensation on the HBT Chaoticity parameter. There are many other effects, such as Coulomb interaction, that may influence the chaoticity parameter measurements in experiments. Further investigations of the other effects on λ measurements to separate out the effect of Bose-Einstein condensation on pion momentum spectrum and HBT measurements in two-pion and multi-pion interferometry will be of great interest.

Acknowledgments

This research was supported by the National Natural Science Foundation of China under Grant No. 11275037.

-
- [1] M. Gyulassy, S. K. Kauffmann, and L. W. Wilson, *Phys. Rev. C* **20** (1979) 2267.
 - [2] Cheuk-Yin Wong, *Introduction to High-Energy Heavy-Ion Collisions*, World Scientific Publishing Company, Singapore, 1994, Chap. 17.
 - [3] U. Wiedemann, U. Heinz, *Phys. Rep.* **319** (1999) 145.
 - [4] R. M. Weiner, *Phys. Rept.* **327** (2000) 249.
 - [5] M. A. Lisa, S. Pratt, R. Soltz, and U. Wiedemann, *Ann. Rev. Nucl. Part. Sci.* **55** (2005) 357.
 - [6] C. N. Fowler and R. M. Weiner, *Phys. Lett. B* **70** (1977) 201; C. N. Fowler and R. M. Weiner, *Phys. Rev. D* **17** (1978) 3118; C. N. Fowler, N. Stelte, and R. M. Weiner, *Nucl. Phys. A* **319** (1979) 349.

- [7] S. Pratt, Phys. Lett. B **301** (1993) 159.
- [8] T. Csörgő and J. Zimányi, Phys. Rev. Lett. **80** (1998) 916; J. Zimányi and T. Csörgő, Acta Phys. Hung. New Ser. Heavy Ion Phys. **9** (1999) 241.
- [9] Cheuk-Yin Wong and Wei-Ning Zhang, Phys. Rev. C **76** (2007) 034905.
- [10] H. D. Politzer, Phys. Rev. A **54** (1996) 5048.
- [11] M. Naraschewski and R. J. Glauber, Phys. Rev. A **59** (1999) 4595.
- [12] J. Viana Gomes, A. Perrin, M. Schellekens, D. Boiron, C. I. Westbrook, and M. Belsley, Phys. Rev. A **74** (2006) 053607.
- [13] J. Liu, P. Ru, and W. N. Zhang, Int. J. Mod. Phys. E **22** (2013) 1350083.
- [14] B. Abelev et al. (ALICE Collaboration), Phys. Rev. C **89** (2014) 024911.
- [15] H. Boggild et al. (NA44 Collaboration), Phys. Lett. B **455** (1999) 77; I. G. Bearden et al. (NA44 Collaboration), Phys. Lett. B **517** (2001) 25.
- [16] M. M. Aggarwal et al. (WA98 Collaboration), Phys. Rev. Lett. **85** (2000) 2895.
- [17] J. Adams et al. (STAR Collaboration), Phys. Rev. Lett. **91** (2001) 262301.
- [18] U. Heinz and P. Kolb, Nucl. Phys. A **702** (2002) 269.
- [19] H. J. Yin, J. Yang, and W. N. Zhang, Phys. Rev. C **86** (2012) 024914.